# Computational Fluid Dynamics Nose-to-Tail Capability: Hypersonic Unsteady Navier-Stokes Code Validation

Thomas A. Edwards* and Jolen Flores†
*NASA Ames Research Center, Moffett Field, California 94035*

**Computational fluid dynamics (CFD) research for hypersonic flows presents new problems in code validation because of the added complexity of the physical models. This paper surveys code validation procedures applicable to hypersonic flow models that include real-gas effects. The current status of hypersonic CFD flow analysis is assessed with the compressible Navier-Stokes code as a case study. The methods of code validation discussed go beyond comparison with experimental data to include comparisons with other codes and formulations, component analyses, and estimation of numerical errors. Current results indicate that predicting hypersonic flows of perfect gases and equilibrium air are well in hand. Pressure, shock location, and integrated quantities are relatively easy to predict accurately, whereas surface quantities such as heat transfer are more sensitive to the solution procedure. Modeling transition to turbulence needs refinement, although preliminary results are promising.**

## Introduction

NATIONWIDE, efforts are underway to develop computational fluid dynamics (CFD) capabilities for problems in hypersonic flight. Forthcoming applications include the National Aero-Space Plane (NASP),[1] high-speed civil transports,[2] aeromaneuvering vehicles, and interplanetary probes. Because of the severe aerothermodynamic environment associated with hypersonic flight, experimental activity is limited. Flight testing is too risky, and ground-based test facilities generally cannot simulate actual flight conditions. Analytical methods developed in the past are useful for preliminary design studies but do not resolve the details of the flowfield sufficiently to provide physical insight into performance trends. CFD has the potential to answer many of these issues, but at the present, capabilities are somewhat limited in terms of physical complexity or geometric generality.

Insofar as the Navier-Stokes equations provide a starting point of modeling hypersonic flows, two solution strategies are widely used. The first is the parabolized Navier-Stokes (PNS) formulation, wherein the governing equations are modified to permit a space-marching solution procedure. This results in a solution capability that is computationally very efficient[3,4] and yields accurate results for a wide variety of geometries and flight conditions. However, PNS equations cannot model flows with streamwise separation or large subsonic regions; therefore, the time-dependent form of the Navier-Stokes equations is used to solve this class of problems, albeit at much greater computational expense. In this approach, an unsteady flow solution is calculated from an initial guess of the flowfield (usually freestream) until a steady-state solution is obtained.

Regardless of the solution method, Navier-Stokes CFD methods provide only a first approximation to hypersonic flow phenomena. The high energy associated with hypersonic flows causes the thermodynamic behavior of air to diverge from the ideal gas assumption applicable at lower speeds. Several modes of internal energy are excited, chemical reactions occur, and radiative heat transfer becomes important at hypersonic conditions. To model these real-gas effects, enhanced physical models[5-7] must be incorporated into CFD codes. Modeling air in chemical equilibrium can be accomplished by incorporating tables or curve fits[8] of thermodynamic properties, but to solve flows in chemical, and possibly thermal nonequilibrium, requires coupling a set of species conservation equations to the fluid dynamic equations. The appropriate equation set to model chemically reacting flows is not universally agreed upon, and in fact it depends on the details of a particular problem.

As with code development efforts for subsonic and transonic CFD in the past, validating numerical hypersonic flow calculations is an integral part of research activity at this time. However, verifying the accuracy of hypersonic calculations is complicated by a narrow data base of flight and experimental measurements. Also, the acute sensitivity of hypersonic vehicle performance to flow parameters requires an unprecedented level of accuracy in the CFD results.

This paper discusses the effort to develop and verify a time-dependent Navier-Stokes formulation with enhanced physical models for nonideal gas properties. Past code validation procedures are reviewed, and new code validation criteria are introduced specifically for hypersonic calculations. The current status of hypersonic CFD capabilities is assessed. Finally, a code validation case study is presented for the compressible Navier-Stokes (CNS) code being developed by the NASA Ames Research Center.

## Elements of Code Validation

For design applications, CFD codes must be able to predict flowfields reliably and accurately over a range of parameters related to vehicle performance. Transonic airfoil applications, for example, need to predict surface pressure coefficients over a range of Mach and Reynolds numbers and angles of attack. Before a CFD code can be used for design applications, it must first be calibrated with existing data to establish its accuracy. Other sources of error must also be quantified: geometrical definition, grid resolution, convergence level, and dissipation, to name a few.

Presented as Paper 89-1672 at the AIAA 24th Thermophysics Conference, Buffalo, NY, June 12-14, 1989; received July 11, 1989. 

*Assistant Chief, Applied Computational Fluids Branch.
†Research Scientist.

Holst[9] recently completed an extensive assessment of CFD codes for transonic airfoil applications. A comparison of nearly two dozen codes on three different airfoils at several flow conditions indicated that the codes do very well predicting the pressure coefficient for attached and moderately separated cases, although the capability is not as mature for flows with large separated regions. The thin-layer Navier-Stokes equations provide a good physical model for these flow conditions, although the turbulence model still needs refinement.

Hypersonic prediction codes feature added complexity beyond transonic codes. This physical phenomena are altogether different: the presence of strong shock waves, high temperatures and heat transfer rates in the boundary layer, chemical and thermal nonequilibrium, and limited upstream influence of flow properties. The physical models in hypersonic CFD codes are also more complex, with the inclusion of species conservation equations, reaction rate equations, fluid/chemistry coupling, and high-temperature transport property models.

The performance of hypersonic flight vehicles depends on a new set of parameters as well. A scramjet-driven vehicle, for example, depends on capturing the shock layer on the windward side of the vehicle to maximize mass flow through the engine. Thus, predicting the shock location and velocity profile in the shock layer assumes importance. For aeromaneuvering vehicles, radiative heat transfer must be accounted for in the energy balance.

The numerous hypersonic CFD codes currently being developed need to be validated to establish their range of applicability for these types of applications. Ideally, this would be accomplished by comparing the calculations with experimental data. But the hypersonic data base is too limited to rely on it as the only means of code validation. Force/moment data and schlieren photographs do not supply sufficient details of the flowfield. Surface pressure data provide a good starting point, but pressure is relatively insensitive to physical models at hypersonic speeds. Heat transfer and skin friction data are much more illustrative of flow inaccuracies. Comparing these quantities indicates how well the viscous flow near the surface is modeled, particularly with regard to the state of the boundary layer. Nonetheless, the state of the boundary layer is often an issue in interpreting experimental measurements of these quantities.

Fortunately, some alternatives that help establish the quality of CFD solutions are available.

1) Code-to-code comparison. This practice will be especially important for nonequilibrium flows because experimental uncertainty often leaves the data only marginally useful. Code-to-code comparison helps quantify numerical errors between algorithms when identical physical models are solved with different methods.

2) Temporal and spatial resolution analysis. Since time-dependent Navier-Stokes formulations seek an asymptotic solution, monitoring relevant flow quantities as the solution is carried forward in time can indicate useful convergence criteria, such as global mass conservation. Obtaining solutions on successively finer grids reduces the numerical truncation error and will quantify the effect of grid resolution errors on flow quantities of interest.

3) Global conservation assessment. Many hypersonic vehicle performance parameters are sensitive to the mass flux. Calculating the global error in mass conservation for the solution domain indicates the uncertainty in quantities derived from mass flux, such as inlet mass capture.

Exploring all available avenues of code validation will insure that CFD results are treated in a manner consistent with their accuracy. Some of these techniques will be demonstrated with the code in development by the NASA Ames Research Center.

## Compressible Navier-Stokes Code Development Effort – Current Status

Part of the NASP Technology Maturation Plan calls for developing a CFD capability for the complete internal/external flow about a hypersonic vehicle with an air-breathing propulsion system. The nose-to-tail effort, as it is called, is being pursued in parallel by government and industry. This section outlines the development of the compressible Navier-Stokes code toward a nose-to-tail capability.

To be instrumental in the NASP design process, the CNS code will not only need the capability to model accurately the different flow regimes and handle complex geometries, but it must also be cost efficient. With this in mind, the CNS code is being developed with a versatile zonal capability that not only simplifies grid generation for complex geometries but also enables solutions to be obtained in a cost-efficient manner. Typically, a complex geometry may require about 10 zones: five viscous streamwise zones and five inviscid zones (wrapped around the viscous zones). This zonal philosophy allows the grid points to be distributed in an efficient manner, that is, the viscous zones may contain as many as 50,000 grids points to capture the relevant flow properties, whereas the inviscid zones may require only 3000 grid points.

Other benefits of the zonal philosophy are that different equation sets can be used where appropriate. For example, the finite-rate chemistry option of the code will be used in those viscous zones near the nose as needed, whereas the equilibrium capability will be used further downstream. In the outer inviscid zones, it may be necessary to solve only the Euler equations. Lastly, convergence acceleration techniques can be used for the different equation sets as well as for new algorithms implemented in appropriate zones.

The CNS procedure to obtain a nose-to-tail solution will be as follows: First a solution will be obtained up to the inlet face using the appropriate options of the code. Then the combustion option of the code (currently under investigation) will solve the internal flow. At the exit plane of the combustion region, the solution would then be continued downstream using the nozzle capability. The results presented in this paper will illustrate those capabilities that are currently implemented in the CNS code. Some options have been thoroughly validated; other options are in the preliminary stages with results that give encouraging qualitative answers.

The CNS code is an extension of the transonic Navier-Stokes (TNS) code developed by Holst et al.[10] The TNS code solves the thin-layer, time-dependent, Reynolds-averaged Navier-Stokes equations. The solution is advanced in time with an implicit, approximately factored algorithm.[11] The original solution algorithm for CNS has been validated with several transonic experiments, including an isolated wing[12] and the full F-16 configuration.[13,14]

To extend the range of applicability to the hypersonic regime, the CNS code incorporates a partially flux-split algorithm,[15,16] which offers improved shock capturing for the strong stocks present in hypersonic flowfields. The Baldwin-Lomax turbulence model[17] provides closure for turbulent flow calculations, and inclusion of a transition model[18] is in progress.

The most significant enhancement of CNS to extend its capabilities to the hypersonic regime has been to incorporate the effects of nonideal gas behavior. As a first approximation, a model for air in chemical equilibrium[8] has been coupled to the CNS flow solver. This approximation is appropriate for a wide range of hypersonic flow applications, especially at relatively low altitudes (compared to re-entry conditions) where the density is high enough that reaction rates are not collision limited. The equilibrium air model consists of a set of curve fits to the thermodynamic and transport properties of high-temperature air, assuming that the reaction rates are infinite. The model is implemented by evaluating polynomials for the properties of air rather than using the ideal gas law. The computational overhead for this enhancement to the CNS code is about 20%.

The next code refinement, currently in progress, is to model the actual chemical reactions of air as it flows past a body. Unlike the equilibrium air model, this model treats chemical

reactions as processes of finite duration and accounts for convection of the reactants while the reactions take place. A set of species conservation equations of the form

$$\frac{D\rho_i}{Dt} = P_i \tag{1}$$

is solved for $n-1$ species, where $n$ is the total number of species being modeled, $i$ is a particular species, $\rho_i$ is the density of $i$, and $P_i$ is a "source" of $i$ resulting from chemical reactions and diffusion. The reaction model implemented in CNS contains six species ($N_2$, $O_2$, NO, N, O, and $NO^+$) plus electrons ($e^-$), which progress through seven reactions:

$$O_2 + M_1 \rightleftharpoons 2O + M_1$$
$$N_2 + M_2 \rightleftharpoons 2N + M_2$$
$$N_2 + N \rightleftharpoons 2N + N$$
$$NO + M_3 \rightleftharpoons N + O + M_3$$
$$NO + O \rightleftharpoons O_2 + N$$
$$N_2 + O \rightleftharpoons NO + N$$
$$N + O \rightleftharpoons O^4 + e^-$$

where $M_x$ are catalytic third bodies. The reaction rates are obtained from Ref. 19. The global continuity equation provides closure for the $n$ species. The initial implementation follows a "loosely coupled" approach,[20] wherein the fluid dynamics equations are solved independently from the chemistry equations. Coupling is achieved by updating the conserved fluid dynamic variables ($\rho$, $\rho u$, $\rho v$, $\rho w$, $e$) with values consistent with the chemical composition after each iteration of the chemistry equations. An alternative formulation is strongly coupled,[21] in that the fluid dynamic and chemistry equations are solved simultaneously. The latter approach is computationally more expensive per time step but may result in more rapid convergence to steady state; further research is needed to resolve this issue.

## CNS Code Validation

This section describes code validation results for the CNS code for the nose-to-tail analysis capability. First, a series of validation studies are presented for the physical models: perfect gas, equilibrium air, nonequilibrium air, and transition to turbulence. Next, calculations for the flow about an external geometry with exhaust nozzle are presented. A detailed component study of the nozzle/afterbody region is also presented to assess predictive capabilities for this important aspect of the nose-to-tail problem. Finally, sources of numerical error are investigated by monitoring the temporal and spatial convergence and global conservation of mass.

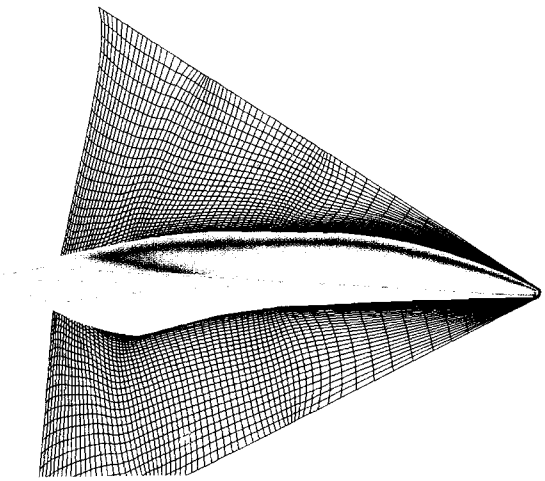

**Fig. 1 Geometry and grid for generic option aerothermal model.**

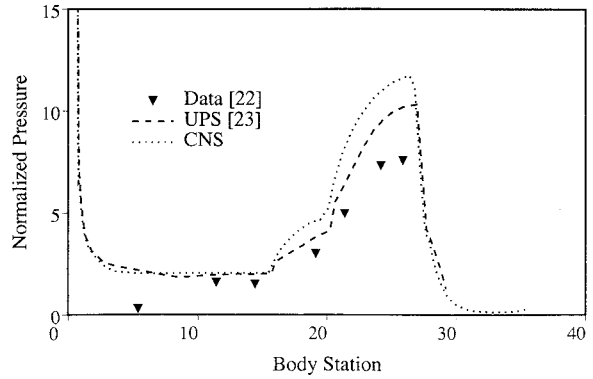


**Fig. 2 Pressure comparisons on windward symmetry plane of generic option at $M_\infty = 11.35$, $\alpha = 0$ deg.**

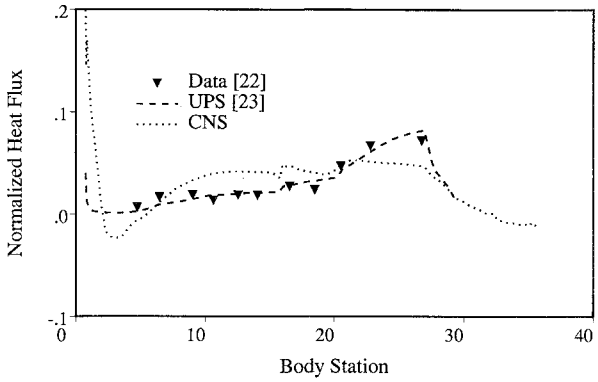


**Fig. 3 Surface heat-transfer comparisons on windward symmetry of generic option at $M_\infty = 11.35$, $\alpha = 0$ deg.**

### Validation of the Physical Models

*Perfect Gas Model*

As a comprehensive check of the CNS code, solutions were obtained for the McDonnell-Douglas generic option blended wing body. Although it is advantageous to use a space-marching method wherever applicable for hypersonic calculations, exercising the CNS code for the entire geometry in this instance enables 1) a checkout of the zonal grid interfacing capabilities, 2) comparisons of the CNS results with those of space-marching method, and 3) creation of a data base for future code enhancement (for example, interfacing the CNS code with space-marching methods).

As Fig. 1 shows, the grid for the generic option consists of eight zones totalling over 350,000 points. A series of four "viscous" zones near the body are arranged in streamwise segments. These zones have grid points highly clustered near the body in the normal direction. Solution of the thin-layer Navier-Stokes equations using the Baldwin-Lomax turbulence model is appropriate for these zones. The Euler equations are solved on the four outer "inviscid" zones, which wrap around the viscous zones and extend to the far field. The resolution of the viscous zones is twice as fine in the circumferential direction and is one-to-one in the streamwise direction relative to the outer zones. Information from an outer zone is transferred to a viscous zone by cubic spline interpolation in the circumferential direction, whereas information is transferred from a viscous zone to an inviscid zone by injection.

The flow conditions for this test case were $M_\infty = 11.35$, $\alpha = 0$ deg, $Re = 31 \cdot 10^6\ m^{-1}$. A perfect-gas equation of state was assumed because the tunnel temperature was not high enough to produce nonideal behavior of the gas. Transition to turbulence was assumed at the nose for the CNS solution. Results were compared with experimental data[22] and a PNS calculation.[23] The PNS calculation employed a transition model that resulted in a transition location at $x/L \approx 0.2$. Com-

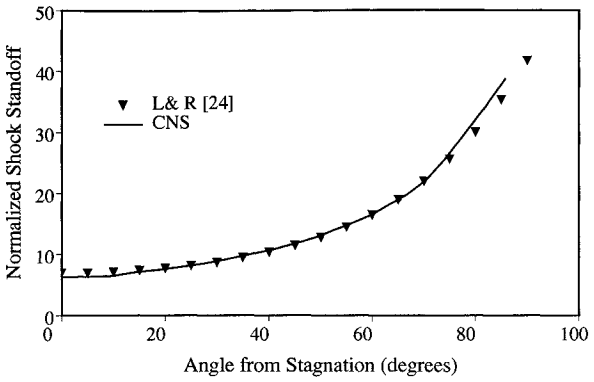


**Fig. 4 Predicted shock location for $M_\infty = 10$ flow past a sphere.**

**Table 1 Comparison of stagnation line quantities for blunt body flow at $M_\infty = 20$**

| Source | $\delta/R_n$ | $P_S/P_\infty$ | $\rho_S/\rho_\infty$ | $P_W/P_\infty$ | $\rho_W/\rho_\infty$ |
|---|---|---|---|---|---|
| CNS | 6.3 | 530.6 | 11.61 | 541.9 | 12.03 |
| Lyubimov and Rusanov[24] | 7.0 | 511.7 | 11.37 | 536.9 | 11.85 |
| Balakrishnan et al.[25] | 7.6 | 509.0 | 11.36 | 531.0 | 11.77 |
| Edwards[26] | 7.2 | 512.0 | 11.29 | 535.0 | 11.80 |

parisons for the windward centerline surface pressure are shown in Fig. 2. The calculated results agree with each other reasonably well, suggesting that the discrepancies with the experimental data are due to a disparity between the calculations and the test conditions.

Figure 3 shows comparisons of the heat transfer rate along the windward centerline. Here, the effect of viscosity (molecular and turbulent) has a strong influence on the results. Whereas the *pressure* at the surface is mostly impressed on the boundary layer from the inviscid flow, the heat transfer rate is strongly influenced by the velocity profile near the wall. The CNS solution shows overall higher heat transfer on the forebody ($0.15 \leq x/L \leq 0.5$) associated with the fully turbulent boundary layer. The predictions are comparable in magnitude, and show some qualitative similarity, but do not lend confidence to current capabilities for complex geometries. The test case chosen here is complicated by 1) an unusual flow pattern on the forebody, discussed in more detail by Lawrence,[23] 2) minor geometrical dissimilarities that had a large effect on the surface flow variables, and 3) the different boundary-layer models applied for the two CFD solutions.

*Equilibrium Air Model*

Including the effects of air in chemical equilibrium widens the solution space of hypersonic flow capabilities considerably. The current model is valid to 25,000 K from densities as low as $10^{-7}$ amagats ($\rho/\rho_0$) up to $10^3$ amagats. To assess the accuracy of the equilibrium air model, two sets of calculations were performed. The first was for a sphere at $M_\infty = 20$, at an altitude of 65,000 ft. Viscous flow results were compared with the inviscid tables of Lyubimov and Rusanov[24] for shock location, pressure, and density. Figure 4 shows that the shock location is predicted reasonably well, although a 10% error near the stagnation streamline is noted. This is thought to be the result of the spherical grid singularity treatment, where solution variables on the axis are obtained by averaging the variables at the nearest adjacent points. This tends to predict a higher pressure jump across the shock relative to the results of Lyubimov and Rusanov. This in turn causes the shock standoff distance on the stagnation streamline to be smaller, as illustrated in Fig. 4. An alternative grid topology is currently under investigation to eliminate the spherical axis singularity.

Table 1 lists other comparisons of the sphere case vs the work of Lyubimov and Rusanov. Balakrishnan et al.[25] ran the shock-fit ARC3D code in the inviscid mode. The predicted pressure was lower by about 0.6%, and hence the shock standoff distance was greater than the work by Lyubimov and Rusanov. Edwards[26] ran the same shock-fit ARC3D code in the viscous mode and his comparisons were in excellent agreement. Notwithstanding the error in the stagnation region noted previously, the equilibrium air model does a good job of predicting the pressure and density jumps across the shock.

The second validation case consisted of a sphere-cone geometry at $M_\infty = 19.24$, $\alpha = 0$ deg, $Re = 93{,}200\ \text{m}^{-1}$, $T_\infty = 182.0$ K, $T_w = 2000$ K, and at an altitude = 275,000 ft. This geometry has a cone angle of 6 deg, a nose radius of 0.152 cm, and a body length of 13.70 cm. Comparisons with previously calculated results of Bhutta et al.[27] are shown in Figs. 5 and 6. The two methods appear to predict pressure nearly identically, although there is some discrepancy in the heat-transfer results near the sphere-cone junction, and the CNS values are lower than the results of Bhutta et al. overall. The CNS results may be influenced by the stagnation point grid singularity, as mentioned previously, because much better agreement has been obtained for similar solutions at angle of attack.[28]

*Finite-Rate Air Chemistry*

As cited previously, the CNS code must have available the option to model flows in chemical nonequilibrium. This option is currently available in the CNS code, although the results that will be shown are preliminary in nature and qualitative at best. Inclusion of the finite-rate air chemistry is done in a "loosely coupled" manner. This allows generality in the solution algorithms for the fluid dynamic and chemistry equations. The solution procedure is as follows: 1) an ideal-gas solution is first obtained, 2) the solution is updated by solving the chemistry equations with the species production terms set to zero (frozen flow), and 3) using the frozen flow as an initial

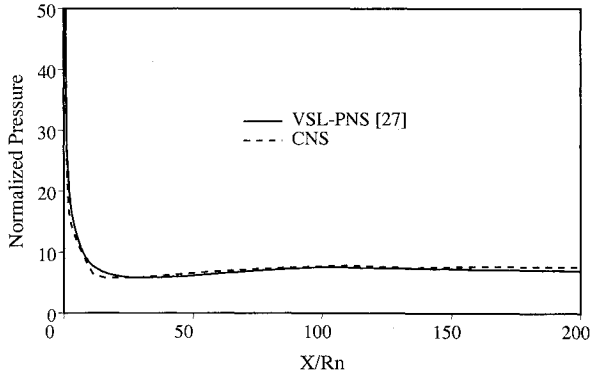


**Fig. 5 Comparison of predicted pressure on a 6-deg cone at $M_\infty = 19.24$, $\alpha = 0$ deg.**

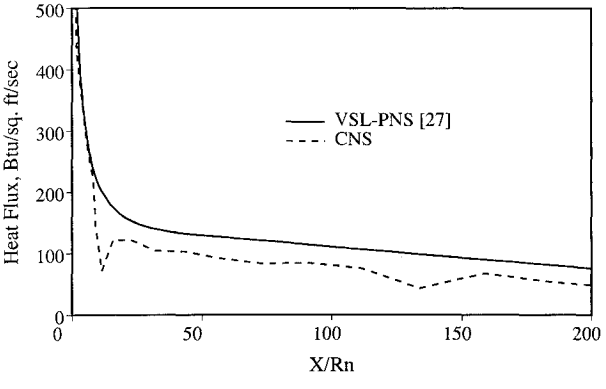


**Fig. 6 Comparison of predicted heat transfer on a 6-deg cone at $M_\infty = 19.24$, $\alpha = 0$ deg.**

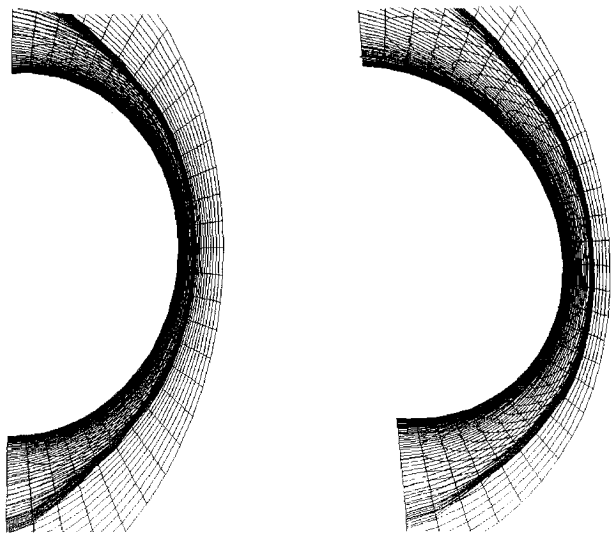

**Fig. 7 Temperature contours for $M_\infty = 10$ flow past a sphere with perfect gas and frozen flow assumptions.**

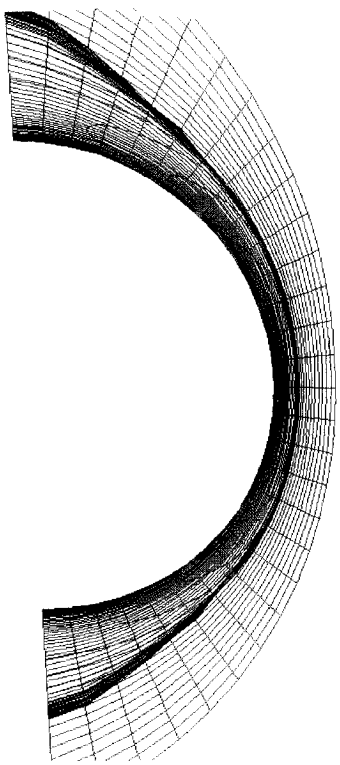

**Fig. 8 Contours of isentropic exponent ($\gamma$) for frozen flow at $M_\infty = 10$ past a sphere.**

guess, the nonequilibrium flow is obtained. This procedure allows a comparison of the flow fields for the perfect gas, frozen flow, and nonequilibrium cases.

For the test case, the freestream conditions were $M_\infty = 10.0$, $\alpha = 0.0$ deg, $T_\infty = 252$ K, $T_w = 1200$ K, and laminar flow. The geometry was a unit sphere with 15 grid points in the streamwise and circumferential directions and 45 grid points in the normal direction. Figure 7 illustrates a symmetry view of the temperature contours for both the perfect gas and frozen (fixed composition, variable $\gamma$) cases. The peak temperature behind the shock for the perfect gas can be seen to be about 5600 K, whereas in the frozen case the peak temperature is about 3400 K. Vibrational and electronic excitation, dissociation, and ionization processes absorb energy and thereby cause the temperature to be lower than in a perfect gas. This results in a higher density jump across the shock and causes the shock to lie closer to the body. Figure 8 is a contour plot of $\gamma$ (isentropic exponent) shown on the symmetry plane. The value of $\gamma$ is 1.4 outside the bow shock, as expected. As the air traverses the shock, the temperature rises, changing the values of the specific heat of air (no longer assumed to be constant). This is turn changes the value of $\gamma$, as can be seen in Fig. 8. The value of $\gamma$ behind the shock drops to a minimum 1.2.

Starting with the frozen solution, an initial guess, the nonequilibrium solution is obtained. Figure 9 is a plot of the mass fraction of $O_2$ and O along the stagnation streamline. The left axis is the magnitude of the mass fraction of $O_2$, and the right axis is the magnitude of O. As the air traverses the shock (at an $x$ value of approximately $-1.07$), the oxygen begins to dissociate, producing atomic oxygen. The degree of dissociation of oxygen and production of atomic oxygen is small, since the temperature behind the shock for these flow conditions is not extremely high. As the flow approaches the cold wall, the backward reaction predominates, as noted in the figure.

Figure 10 illustrates the same trends for the dissociation of molecular nitrogen ($N_2$) to atomic nitrogen. The production of atomic nitrogen, however, is orders of magnitude smaller than that of oxygen. This is to be expected, since the activation energy needed to dissociate $N_2$ is much higher than that for $O_2$.

### Laminar-Turbulent Transition

The turbulence transition model implemented in CNS requires that the transition criterion, $Re_\theta$, be prescribed. Typical values of $Re_\theta$ range from 100 to 400, depending on the geometry and flow conditions, and so some calibration is necessary. The test case considered here is a sharp-nosed, 8-deg half-angle cone at $M_\infty = 10$, $\alpha = 0$ deg based on an experiment by Di-Cristina.[29] The transition criterion was specified by correlating the onset of transition in the experiment with previously calcu-

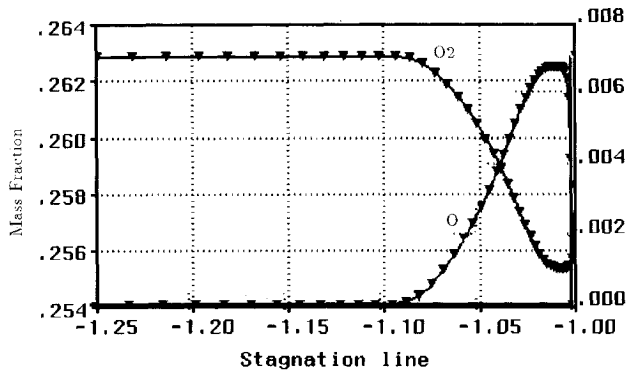


**Fig. 9 Stagnation line mass fractions of molecular and atomic oxygen for chemically reacting $M_\infty = 10$ flow past a sphere.**

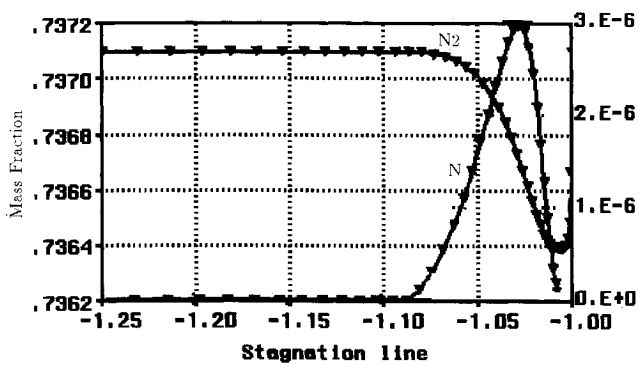


**Fig. 10 Stagnation line mass fractions of molecular and atomic nitrogen for chemically reacting $M_\infty = 10$ flow past a sphere.**

lated results. Surface heat transfer, a quantity sensitive to the state of the boundary layer, is presented in Fig. 11. The CNS prediction is qualitatively similar to the experimental results, bu the heat transfer rate is substantially overpredicted at the end of the transition region. This stems from the fact that the initial implementation of the transition model was designed for space-marching solution methods. The model attempts to acquire the correct turbulent viscosity at the end of the transition region, assuming no upstream influence. As a consequence, time-marching solution produces too much turbulent viscosity in the transition region. Corrections to this model to accommodate time-dependent formulations are in progress.

#### Component Validation-Nozzle/Plume Flow

The underexpanded, chemically reacting exhaust gases leaving the nozzle expand along the vehicle afterbody, which contributes a significant fraction to the total thrust generated by the scramjet engine. Predicting the flow accurately in this region is critical to determining thrust requirements and engine performance. As a first approximation, a frozen chemistry model has been implemented in an upwind, time-dependent Navier-Stokes formulation[30] to model the exhaust gases as a separate species from the external flow. Extensive validation calculations have been carried out for a nozzle/afterbody test model.[31] In this test, the exhaust gas had an isentropic exponent $\gamma$ of 1.26 and the external flow was air ($\gamma = 1.4$). The model was tested at Mach 6 for a series of exit pressure ratios.

For example, comparisons of the measured and calculated surface pressure coefficients are shown in Fig. 12. The expansion process is predicted well, although the calculation fails to predict the pressure peak on the plate near the nozzle exit station. To improve the correlation, velocity profiles at the exhaust nozzles are needed, along with better grid resolution in the initial plume expansion region, as detailed in Ref. 31. Nonetheless, these preliminary results are promising for flow predictions of nozzle/afterbody flows.

#### Validation of Numerical Convergence

*Temporal Convergence*

Time-dependent solutions of steady flows solve the unsteady evolution of a flowfield (usually *not* time accurately) from an initial guess until the solution is independent of the time step. The solution algorithm for the CNS code has the form

$$\mathcal{L}\Delta Q^n = \mathcal{R} \tag{2}$$

where $\mathcal{L}$ is the implicit operator, $\Delta Q^n$ the correction to the solution vector at the current "time" step $n$, and $\mathcal{R}$ the residual, effectively an evaluation of the partial differential equations using the current solution. The equation is solved exactly when $\mathcal{R} = 0$. Hence, a commonly used convergence criterion is the $L_2$-norm of the residual $\mathcal{R}$, where $N$ is the total number of grid points in the domain.

$$\|\mathcal{R}\|_2^n = \left\{\frac{1}{N}\sum_{i=1}^{N}[\mathcal{R}^n(i)]^2\right\}^{1/2} \tag{3}$$

The solutions presented here were, for the most part, obtained from a three-order-of-magnitude reduction in the $L_2$-norm of the residual from its maximum value. However, other quantities may be equally indicative of convergence: global mass conservation, lift, drag, or skin friction, for example.

In Fig. 13, the convergence history for a blunt body flow at $M_\infty = 11.35$ is shown. Several features of this plot are noteworthy. First, the $L_2$-norm of the overall residual is dominated by the residual of the energy equation, since each of the other residuals is at least an order of magnitude smaller. Next, the global mass conservation error exhibits more than one minimum as the solution approaches a steady state. This may be because of fortuitous cancellation of errors, and caution

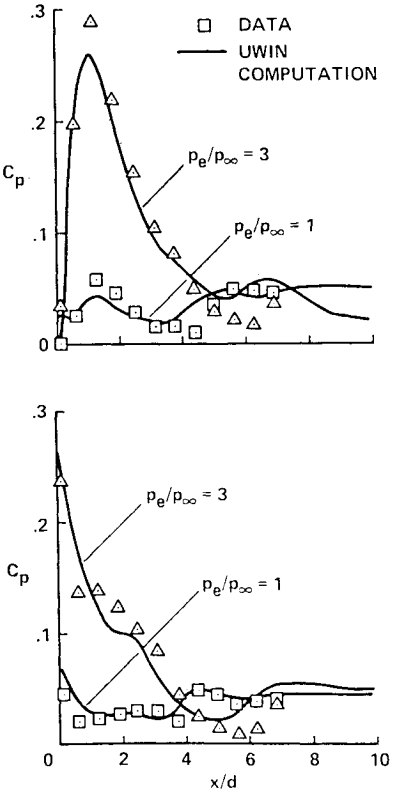


**Fig. 12 Comparison of calculated and measured pressure on surface of nozzle/afterbody model at $M_\infty = 6$, $\alpha = 0$ deg.**

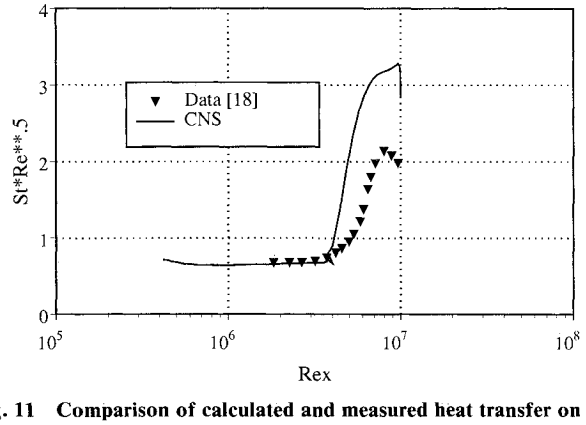


**Fig. 11 Comparison of calculated and measured heat transfer on an 8-deg sharp cone with transitional flow at $M_\infty = 10$.**

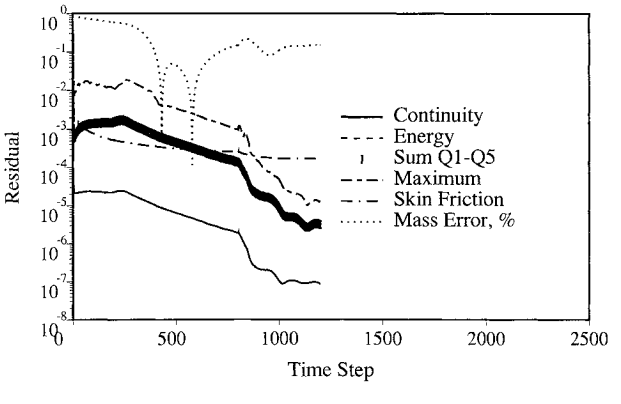


**Fig. 13 Convergence history of various quantities for calculation of $M_\infty = 11.35$ flow past a sphere.**

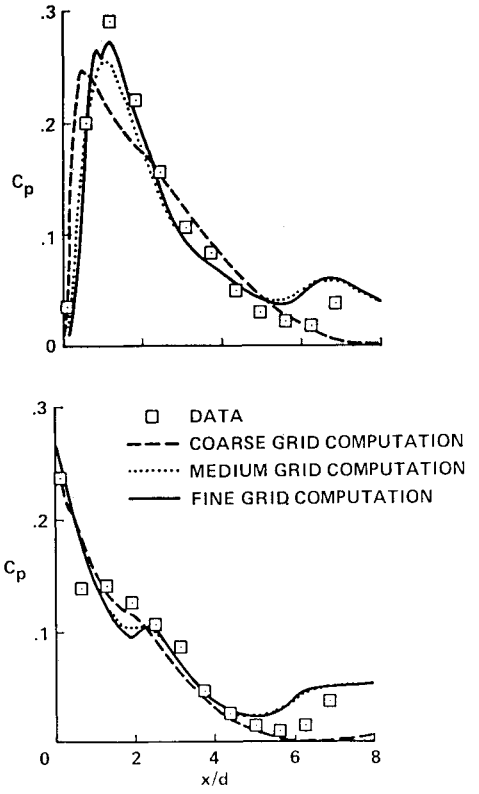


**Fig. 14 Comparison of calculated pressure on surface of nozzle/afterbody model on a succession of grids, $M_\infty = 6$, $\alpha = 0$ deg.**

**Table 2 Comparison of calculated normal force coefficients for nozzle/afterbody model on successively finer grids**

| Grid | Dimensions | Total points | $C_n$ |
|---|---|---|---|
| Coarse | $31\times17\times31$ | 16,337 | 0.1009 |
| Medium | $60\times33\times62$ | 122,760 | 0.1256 |
| Fine | $119\times63\times123$ | 922,131 | 0.1362 |

should be exercised in using this quantity as a convergence criterion. Finally, the $L_2$-norm of skin friction shows a more gradual, though monotone, reduction to its asymptotic value. This characteristic can present difficulty in establishing a cutoff point for convergence. Nonetheless, all the equations generally show acceptable levels of convergence at the end of the calculation.

*Spatial Convergence*

Grid resolution is also an important potential source of error. Coarse grids can completely smear out physical phenomena such as flow separation. Only by obtaining solutions on progressively finer grids, until an asymptotic limit is attained, can the effect of the grid on the solution be eliminated. Figure 14 shows pressure coefficients for the preceding nozzle/afterbody model for three grids of increasing refinement. The results show how the pressure peak is predicted better as the grid resolution increases. In Table 2, the normal force on the plate is seen to reach an asymptotic value with the fine grid, and so further refinement would not be expected to alter the prediction of the normal force. However, other quantities such as heat transfer may still be influenced by further refinement. Whether a flowfield is adequately resolved on a given grid depends on the parameters of interest.

## Conclusions

The complexity of the physical models for hypersonic flows creates unique challenges in validating CFD codes. In most instances, experimental data are inadequate to thoroughly validate the solution method. Thus, other means are necessary to supplement hypersonic code validation. While code validation is necessarily founded on comparison with experimental data, a significant measure of accuracy can also be determined from the solution itself. For example, errors in global mass conservation monitor the uncertainty of many physical quantities deduced from a CFD solution. Hypersonic flow codes need to quantify error estimates before being applied to design problems.

The ongoing development and validation of the CNS code has been described as a case study for calibrating unsteady hypersonic Navier-Stokes codes. Results to date show good performance for both perfect and equilibrium air models. Modeling transition to turbulence shows promise, but needs improvement. The ability of CNS to predict quantities such as heat transfer and skin friction depends on both the level of convergence and the resolution of the grid. Comparisons of CNS results with PNS codes indicate that both approaches give acceptable answers for the attached flows studied here.

Future work on flows in chemical and thermal nonequilibrium will be even more difficult to validate. Covalidation with other CFD results will be relied upon increasingly. Quantifying numerical errors will help insure that results are interpreted accordingly. Thorough code validation is necessary for CFD to make a contribution to designing hypersonic vehicles of the near future.

## References

[1]Howe, J. T., "Introductory Aerothermodynamics of Advanced Space Transportation Systems," *Journal of Spacecraft and Rockets*, Vol. 22, No. 1, 1985, pp. 104-111.

[2]Morris, C. E. K., Jr., Winston, M. M., and Morris, S. J., Jr., "Some Key Considerations for High-Speed Civil Transports,"AIAA Paper 84-4466, 1988.

[3]Vigneron, Y. C., Rakich, J. V., and Tannehill, J. C., "Calculation of Supersonic Viscous Flow over Delta Wings with Sharp Subsonic Leading Edges," AIAA Paper 78-1137, 1978.

[4]Schiff, L. B. and Steger, J. L., "Numerical Simulation of Steady Supersonic Viscous Flow," AIAA Paper 79-0130, 1979.

[5]Candler, G. V., and MacCormack, R. W., "The Computation of Hypersonic Ionized Flows in Chemical and Thermal Nonequilibrium," AIAA Paper 88-0511, 1988.

[6]Park, C., "Assessment of Two-Temperature Kinetic Model for Ionizing Air," AIAA Paper 87-1574, 1987.

[7]Park, C., and Yoon, S., "A Fully-Coupled Implicit Method for Thermo-Chemical Nonequilibrium Air at Sub-Orbital Flight Speeds," AIAA Paper 89-1974, 1989.

[8]Srinivasan, S., Tannehill, J. C., and Weilmuenster, K. J., "Simplified Curve Fits for the Thermodynamic Properties of Equilibrium Air," NASA RP 1181, 1987.

[9]Holst, T. L., "Viscous Transonic Airfoil Workshop Compendium of Results," AIAA Paper 87-1460, 1987.

[10]Holst, T. L., Kaynak, U., Gundy, K. L., Thomas, S. D., Flores, J., and Chaderjian, N. M., "Transonic Wing Flows Using an Euler Navier-Stokes Zonal Approach," *Journal of Aircraft*, Vol. 24, No. 1, 1987, pp. 17-24.

[11]Beam, R., and Warming, R., "An Implicit Finite-Difference Algorithm for Hyperbolic Systems in Conservation-Law Form," *Journal of Computational Physics*, Vol. 22, Sept. 1976, pp. 87-110.

[12]Kaynak, U., and Flores, J., "Advances in the Computation of Transonic Separated Flows over Finite Wings," *Computers and Fluids*, Vol. 17, No. 2, 1989, pp. 313-332.

[13]Flores, J., Chaderjian, N. M., and Sorenson, R. L., "Simulation of Transonic Viscous Flow over a Fighter-Like Configuration Including Inlet," *Journal of Aircraft*, Vol. 26, No. 4., 1989, pp. 295-301.

[14]Flores, J., and Chaderjian, N. M., "The Numerical Simulation of Transonic Separated Flow About the Complete F-16A," AIAA Paper 88-2506, 1988.

[15]Ying, S. X., Steger, J. L., Schiff, L. B., and Baganoff, D., "Numerical Simulation of Unsteady, Viscous, High-Angle-of-Attack Flows Using a Partially Flux-Split Algorithm," AIAA Paper 86-2179, 1986

[16]Rizk, Y. M., Chaussee, D. S., and Steger, J. L., "Numerical Simulation of the Hypersonic Flow Around Lifting Vehicles," NASA TM 89444, 1987.

[17]Baldwin, B. S. and Lomax, H., "Thin-Layer Approximation and

Algebraic Model for Separated Turbulent Flows," AIAA Paper 78-257, 1978.

[18]Kaul, U. K., "Laminar-Turbulent Transition Calculations of Heat Transfer at Hypersonic Mach Numbers over Sharp Cones," *Collected Papers in Heat Transfer 1988*, edited by, K. T. Yang, American Society of Mechanical Engineers, HTD-Vol. 104, 1988.

[19]F. G. Blottner, M. Johnson, and Ellis, M., "Chemically Reacting Viscous Flow Program for Multi-Component Gas Mixtures," Sandia Lab., Albuquerque, NM, Rept. SC-RR-70-754, Dec. 1971.

[20]Balakrishnan, A., "Application of a Flux-Split Algorithm to Chemically Relaxing, Hypervelocity Blunt-Body Flows," AIAA Paper 87-1578, 1987.

[21]Molvik, G. A., and Merkle, C. L., "A Set of Strongly Coupled, Upwind Algorithms for Computing Flows in Chemical Nonequilibrium," AIAA Paper 89-0199, 1989.

[22]"NASP Generic Option No. 2 – CFD Code Validation," McDonnell Douglas, Fourth Quarterly Rept. F33657-86-C-2126, Oct. 1987.

[23]Lawrence, S. L., "(U) Comparison of the UPS Code with Experimental Data for the McDonnell Douglas Generic Option Vehicle," Fifth National Aerospace Plane Technology Symposium, Paper 78.

[24]Lyubimov, A. N., and Rusanov, V. V., "Gas Flows Past Blunt Bodies," NASA TT F-715.

[25]Balakrishnan, A., Davy, W. C., and Lombard, C. K., "Real-Gas Flowfields about Three-Dimensional Configurations," *Journal of Spacecraft and Rockets*, Vol. 22, No. 1, 1985, pp. 46–53.

[26]Edwards, T. A., Unpublished results.

[27]Bhutta, B. A., Lewis, C. H., and Kautz, F. A. II, "A Fast Fully-Iterative Parabolized Navier-Stokes Scheme For Chemically-Reacting Reentry Flows," AIAA Paper 85-0926, 1985.

[28]Ryan, J. S., Flores, J., and Chow, C. Y., "Development and Validation of CNS (Compressible Navier-Stokes) for Hypersonic External Flows," AIAA Paper 89-1839, 1989.

[29]DiCristina, V., "Three-Dimensional Laminar Boundary-Layer Transition on a Sharp 8° Cone at Mach 10," AIAA Paper 69-12, 1969.

[30]Edwards, T. A., "The Effect of Exhaust Plume/Afterbody Interaction on Installed Scramjet Performance," AIAA Paper 89-0082, 1989.

[31]Cubbage, J. M., Jr., and Kirkham, F. S., "Investigation of Engine-Exhaust-Airframe Interference on a Cruise Vehicle at Mach 6," NASA TN D-6060, 1971.

Clark H. Lewis
*Associate Editor*